Modeling of X-ray images and energy spectra produced by stepping lightning leaders

Wei Xu,[1] Robert A. Marshall,[1] Sebastien Celestin,[2] and Victor P. Pasko[3]

Wei Xu and Robert A. Marshall, Department of Aerospace Engineering Sciences, University of Colorado Boulder, Boulder, Colorado 80309, USA (Wei-Xu@colorado.edu; Robert.Marshall@colorado.edu)

Sebastien Celestin, LPC2E, 3A avenue de la Recherche Scientifique, 45071 Orleans Cedex 2, France (sebastien.celestin@cnrs-orleans.fr)

Victor P. Pasko, Communications and Space Sciences Laboratory, Department of Electrical Engineering, Pennsylvania State University, 227 EE East, University Park, PA 16802-2706, USA (vpasko@psu.edu)

[1]Department of Aerospace Engineering Sciences, University of Colorado Boulder, Boulder, Colorado, USA.

[2]LPC2E, University of Orleans, CNRS, Orleans, France.

This article has been accepted for publication and undergone full peer review but has not been through the copyediting, typesetting, pagination and proofreading process, which may lead to differences between this version and the Version of Record. Please cite this article as doi: 10.1002/2016JD026410

Abstract.

Recent ground-based measurements at the International Center for Lightning Research and Testing (ICLRT) have greatly improved our knowledge of the energetics, fluence, and evolution of X-ray emissions during natural cloud-to-ground (CG) and rocket-triggered lightning flashes. In this paper, using Monte Carlo simulations and the response matrix of unshielded detectors in the Thunderstorm Energetic Radiation Array (TERA), we calculate the energy spectra of X-rays as would be detected by TERA and directly compare with the observational data during event MSE 10-01. The good agreement obtained between TERA measurements and theoretical calculations supports the mechanism of X-ray production by thermal runaway electrons during the negative corona flash stage of stepping lightning leaders. Modeling results also suggest that measurements of X-ray bursts can be used to estimate the approximate range of potential drop of lightning leaders. Moreover, the X-ray images produced during the leader stepping process in natural negative CG discharges, including both the evolution and morphological features, are theoretically quantified. We show that the compact emis-

[3]Communications and Space Sciences
Laboratory, Department of Electrical
Engineering, Pennsylvania State University,
University Park, Pennsylvania, USA.

sion pattern as recently observed in X-ray images is likely produced by X-rays originating from the source region and the diffuse emission pattern can be explained by the Compton scattering effects.

1. Introduction

Ground-based detectors have recently revealed that both natural cloud-to-ground (CG) [*Moore et al.*, 2001] and rocket-triggered lightning flashes [*Dwyer et al.*, 2003] are associated with intense bursts of X-ray emissions. Different from the long-duration gamma-ray radiation measured during thunderstorms [e.g., *Chilingarian et al.*, 2010], these X-ray bursts have a typical duration as short as fractions of a microsecond and a characteristic energy spectra extending up to a few MeVs [e.g., *Dwyer et al.*, 2004, 2012]. More detailed studies of this radiation phenomenon have been carried out at the International Center for Lightning Research and Testing (ICLRT) using the Thunderstorm Energetic Radiation Array (TERA) [e.g., *Saleh et al.*, 2009; *Schaal et al.*, 2012] and a pinhole-type high-speed X-ray Camera (XCAM) [e.g., *Dwyer et al.*, 2011; *Schaal et al.*, 2014]. TERA observations have brought important insights into the energetics and brightness of these X-ray emissions. *Schaal et al.* [2012] have shown that X-ray bursts detected during both natural CGs and rocket-triggered lightning discharges can be explained by an electron source with a characteristic energy less than 3 MeV and a maximum production rate of 10^{17} electrons/s.

X-ray images captured by XCAM have provided a novel perspective on the temporal and spatial evolution of X-ray production. By comparing X-ray images with concurrent measurements of nearby electric field derivative waveforms during two triggered lightning events, *Dwyer et al.* [2011] have pointed out that X-ray bursts originate at the tip region of dart leaders. In addition, *Schaal et al.* [2014] have performed detailed analysis on the X-ray structure of triggered lightning discharges and found that lightning leaders exhibit

both diffuse and compact emission patterns in X-ray images, and that the electric charge contained in the X-ray source region, with a radius between 2–3 m, is approximately 10^{-4} C.

Extensive observations have been made by the aforementioned instruments, but the mechanism of X-ray production is still uncertain. The mechanism of relativistic runaway electron avalanches (RREA) [*Gurevich et al.*, 1992] has so far provided a very good agreement with satellite measurements of gamma-ray radiation from intracloud lightning discharges: terrestrial gamma-ray flashes [*Dwyer and Smith*, 2005], and the gamma-ray radiation measured at mountain tops [e.g., *Chilingarian et al.*, 2010]. However, it has been suggested that this mechanism is inconsistent with the energy spectra of X-rays measured during natural CG or triggered lightning flashes [e.g., *Dwyer*, 2004; *Schaal et al.*, 2012; *Arabshahi et al.*, 2015]. Alternatively, *Celestin and Pasko* [2011] have shown theoretically how these X-ray bursts can originate from the bremsstrahlung radiation of thermal runaway electrons produced during the negative corona flash stage of stepping lightning leaders. On the basis of this mechanism, the derived energy spectrum of X-rays resulting from typical −CG stepped leaders, without considering the detector response, has been found to resemble that measured by TERA [*Xu et al.*, 2014]. However, in order to accurately interpret X-ray measurements and unravel the source mechanism, a direct comparison between observed energy spectra and theoretical calculations with the detector response taken into consideration is of critical significance. For this purpose, Monte Carlo simulations are employed in cooperation with the response matrix of unshielded TERA detectors, with the goals to quantify, from first principles, (1) the X-ray energy

spectra as would be recorded by TERA detectors and (2) the X-ray images produced by stepping lightning leaders during natural −CG discharges.

2. Model Formulation

The present work builds on the modeling study of *Xu et al.* [2014] and is developed based on the mechanism of X-ray production by thermal runaway electrons (see *Celestin and Pasko* [2011] and references therein for discussion of related phenomenon). During the negative corona flash stage of stepping lightning leaders, the exponential growth of the potential differences in streamers gives rise to the production of thermal runaway electrons with a characteristic energy of ∼65 keV. These thermal runaway electrons can be further accelerated by the inhomogeneous electric field near the tip region of the lightning leader. First, the method of moments was used to compute the electric field produced near the tip region of −CG lightning leaders. Second, using Monte Carlo models, we simulated the acceleration of thermal runaway electrons in the electric field obtained in the first step and the transport of resultant bremsstrahlung X-rays in the atmosphere. Modeling results of the first two steps have been reported in [*Xu et al.*, 2014] and are directly used in this work. Finally, the energy spectra are derived from Monte Carlo simulations with the knowledge about the response function of TERA detectors for incident X-rays. By calculating the incident angles of photons with respect to the detector surface, we further quantify the X-ray image. The simulation domain used for modeling X-ray images, as well as accelerating thermal runaway electrons in the lightning leader field and the trajectories of those X-rays that arrive at ground-based detectors, are schematically depicted in Figure 1a. Black dots in this figure denote the locations where Compton scatterings by air molecules take place.

The key parameter of this study is the potential drop formed in the tip region of lightning leaders (named "potential drop" in the following for simplicity). It specifically refers to the potential difference between the leader tip and the ambient potential at the leader tip. Note that the potential drop defined herein is only a fraction of the potential difference between the lightning leader tip and the ground. Typical values for the potential difference between a downward-moving stepped-leader tip and ground are on the order of some tens of megavolts [e.g., *Rakov and Uman*, 2003, p. 111]. Therefore, an order of magnitude estimate for the potential drop in the tip region of stepped leaders would be ∼10 MV [*Bazelyan and Raizer*, 2000, p. 163]. For lightning leaders with a potential drop of a few tens of MV, thermal runaway electrons (seed electrons in the present work) do not avalanche significantly following the RREA process and the corresponding energy distribution does not exhibit the characteristic high-energy cutoff (7 MeV), as typical of RREAs. For these reasons, the RREA process is not fully developed in the present study of X-ray production during natural −CG discharges.

In the present work, we mainly investigate lightning leaders with a potential drop of 10 MV in the tip region. This value is chosen because it is representative, as an order of magnitude estimate, for stepped leaders in −CGs [*Bazelyan and Raizer*, 2000, p. 163]. Additionally, *Xu et al.* [2014] have modeled the X-ray emissions by lightning leaders with two potential drops: 5 MV and 10 MV. The most energetic X-rays arising from the 10 MV leader are more consistent with those measured at ground level, when compared with the 5 MV leader. For the sake of comparison with TERA-measured X-ray spectra (Figure 1b), we have also simulated the X-ray production by lightning leaders with a potential

drop of 50 MV. The potential drop of 10 MV represents common lightning leaders in −CGs, while 50 MV represents extremely energetic ones.

We use the method of moments [*Balanis*, 1989, p. 670] in order to calculate the electric field produced in the vicinity of a −CG lightning leader tip. Briefly, the lightning leader is assumed to be an equipotential and perfectly conducting cylinder that is aligned with the ambient large-scale electric field in the thunderstorm. The polarization of the leader in the ambient field would result in a specific charge distribution. The method of moments [*Balanis*, 1989, p. 670] is used to convert Maxwell's equations into a set of matrix equations in the volume of interest and to solve the electric charge distribution induced on the channel. Knowing the charge distribution, this method allows for reconstructing the three-dimensional electric field configuration near the negative end of the leader channel. The potential difference between the leader tip and the ambient potential is approximately $U_l = E_0 l/2$ [*Bazelyan and Raizer*, 2000, p. 54], where E_0 is the ambient large-scale thunderstorm electric field and l is the length of the unbranched leader channel. We have studied lightning leaders with two potential drops: $U_l = 10$ MV ($E_0 = 0.2$ kV/cm, $l = 1$ km) and $U_l = 50$ MV ($E_0 = 0.5$ kV/cm, $l = 2$ km). In both cases, the radius of the leader channel is chosen as 1 cm [*Rakov and Uman*, 2003, Section 4.4.6, p. 134].

We emphasize that the specific choices of these physical parameters would not significantly change present modeling results as long as the resultant potential drop is the same. A constant value is chosen for E_0 because it allows straightforward physical interpretation of the potential drop and direct calculation of the electric field near the tip region. Note that thermal runaway electrons produced during the negative corona flash stage are assumed to have a characteristic energy of ∼65 keV [*Celestin and Pasko*, 2011]. The

dynamic friction force for these electrons is approximately 6.4 keV/cm at ground level air density [e.g., *Moss et al.*, 2006, Figure 2]. Therefore, an ambient electric field with a magnitude equal to or slightly larger than the RREA threshold electric field (defined for minimum ionizing electrons) is incapable of overcoming the collisional energy loss that thermal runaway electrons experience.

The Monte Carlo model employed for simulating the propagation and collisions of electrons in air is similar to that described in *Celestin and Pasko* [2011]. The model is three-dimensional (3-D) in the velocity space, 3-D in the configuration space, relativistic, and simulates electrons with energies from sub-eV to GeV. In order to avoid the acceleration of electrons in unphysically high electric fields [e.g., *Celestin and Pasko*, 2011], the initial location of thermal runaway electrons is set at 15 cm and 80 cm from the leader tip for the potential drop of 10 MV and 50 MV, respectively. The Monte Carlo model developed to simulate photon transport in the Earth's atmosphere is similar to that described in *Østgaard et al.* [2008]. Three main collision types for photons with energies between 10 keV and 100 MeV are considered: photoelectric absorption, Compton scattering, and electron-positron pair production. We emphasize that the set of Monte Carlo models has been validated through calculations of TGF energy spectra based on the RREA theory and a very good agreement has been obtained with previous published results [*Dwyer and Smith*, 2005; *Celestin et al.*, 2012; *Xu et al.*, 2012, 2015].

As lightning leader propagates towards the ground, the potential drop formed in the tip region may undergo significant changes. The leader tip approaching the ground is associated with a three dimensional network of leaders extending from many kilometers above, which also spread for several kilometers horizontally [*Bazelyan and Raizer*, 2000].

In the present work, we assume that the potential drop at the leader tip remains constant during subsequent steps and use the following additional simplifications. First, lightning leaders propagate vertically downward towards the ground (see Figure 1a) in a series of discrete steps [*Bazelyan and Raizer*, 2000, p. 84] and X-rays are emitted solely after the establishment of a new leader step [*Dwyer et al.*, 2005]. The length of leader steps is chosen to be 10 m and 20 m [e.g., *Rakov and Uman*, 2003; *Tran et al.*, 2014; *Qi et al.*, 2016] for the potential drop of 10 MV and 50 MV, respectively. Note that the step length is only used in the calculation of X-ray energy spectrum (Figure 1b) and energy deposition (Figure 1c). Second, it is assumed that the potential drop formed in the leader tip region is invariant during the stepping process. Considering that the energy distribution of bremsstrahlung photons is mainly controlled by the potential drop [*Celestin et al.*, 2015], we also assume that X-ray bursts emitted at each leader step follow the same energy distribution as would be produced by the 10 MV [e.g., *Xu et al.*, 2014, Figure 2] or 50 MV lightning leader. The angular distribution of these X-rays is assumed to be isotropic within a downward solid angle of 2π, as suggested by *Saleh et al.* [2009].

Concerning the spatial distributions of source X-rays, it is assumed that they are uniformly produced within a hemisphere centered at the leader tip, representing the associated streamer zone [e.g., *Xu et al.*, 2014]. The radius of the streamer zone can be estimated using its proportionality with the potential drop of lightning leaders [e.g., *Celestin and Pasko*, 2011; *Bazelyan and Raizer*, 2000]. The values for lightning leaders with potential drops of 10 MV and 50 MV are 4 m and 20 m, respectively. However, it is difficult to estimate theoretically the number of high-energy photons produced by a lightning leader. As pointed out by *Celestin et al.* [2015], the number of photons with energies greater than 10

keV produced by a typical −CG stepped leader is expected to be on the order of 10^{11}–10^{12} (see *Celestin et al.* [2015] and references therein for discussion of related derivation).

In the present modeling of leader stepping process, we have not considered the effects of ground proximity and leader branching. The effect of ground proximity could enhance the electric field produced near the tip region of lightning leaders and the effect of leader branching could lower the electric potential that stepping leaders transport down to the ground. In principle, different lightning leaders approaching the ground may form various potential drops with various time dynamics. In the present work, we consider a greatly simplified system with a unique time-independent magnitude of the potential drop. The results obtained using this assumption are presented and discussed in the following sections.

The dynamics of lightning leaders is fundamentally different between natural −CG discharges and triggered lightning and, in this study, we focus on natural −CGs. The X-ray emissions measured at ground level during −CGs are intrinsically different from the long-duration gamma-ray fluxes measured at mountain tops [*Chilingarian et al.*, 2010] in terms of total duration and energy spectra [e.g., *Dwyer et al.*, 2012]. Because of these differences, we only investigate the submicrosecond X-ray bursts recorded at ground level by TERA. Among previously published TERA measurements, energy spectrum has only been reported for one −CG event: MSE 10-01 [*Schaal et al.*, 2012, Figure 10]. MSE 10-01 was measured by the Multiple Station Experiment (MSE) on June 30, 2010 at ICLRT. As explained in [*Schaal et al.*, 2012], "MSE refers to a natural flash and is followed by the year", e.g., 10 for 2010, "and the flash number", e.g., 01. The stepped leader in this event had an average speed of 4.22×10^5 m/s [e.g., *Schaal et al.*, 2012] and *Schaal et al.*

[2012] have reported TERA measurements of X-ray radiation 891 μs prior to the time of the return stroke. X-ray bursts were recorded during the propagation from approximately 376 m altitude to the ground. This range of altitudes and the leader speed are adopted herein as a reference in the modeling of the stepping process.

For the sake of direct comparison with TERA measurements, we spatially average the energy spectra obtained in our simulations at given radial distances from the burst location using the distribution of TERA stations [*Schaal et al.*, 2012, Figure 4]. This technique is based on the assumed radial symmetry of the system and largely increases the statistics of modeling results at a given radial distance. In particular, the first step of spectra calculation is collecting photons that arrive at ground level using concentric rings with a horizontal width of 100 m between the inner and outer radius, up to a radial distance of 500 m from the lightning ground impact location. Second, for each collecting ring, the energy distribution of photons is calculated and normalized to unity. The spatially averaged energy distribution is further derived by summing over the energy distributions weighted by the density of detectors contained within each ring. Finally, the X-ray energy spectra that would be measured by TERA are obtained by folding the averaged energy distribution with the response matrix of unshielded TERA detectors. The formulas used for the calculation of energy deposition [*Arabshahi et al.*, 2015] and the convolution of the photon energy distribution with the detector response matrix are presented in Appendix A.

In the present work, we model an X-ray camera with an elevation angle of 45° and a minimum energy threshold of 30 keV [*Dwyer et al.*, 2011] for two locations: 44 m and 150 m horizontally from the lightning ground impact location. More precisely, we accumulate

photons at ground level over concentric rings at radial distances between 43 and 45 m, and 149 and 151 m for the locations of 44 m and 150 m, respectively. The X-ray images are simulated using 88×88 numerical grid points (i.e., pixels) for a field of view between ±44° in both vertical and horizontal directions, providing an angular resolution of 1°×1°. Note that, different from the X-ray camera modeled in the present study, the field of view for XCAM is ±38° in vertical and horizontal directions, with an angular resolution of 4° to 8°, and XCAM was pointed at the lightning channel with an elevation angle of 49° during the event reported in [*Dwyer et al.*, 2011]. Future measurements can be compared with present results by integrating the simulated X-ray images with the knowledge about the angular resolution of the instrument used. In order to investigate the Compton scattering effects and the evolution of X-ray images, X-ray images are calculated for leader steps at a few representative altitudes close to the ground.

For each photon collected within the concentric ring, we assume that the photon is detected by an above-mentioned X-ray camera that is pointed at the lightning channel. The normal vector of the detector surface and the instrument field of view in vertical and horizontal directions are first identified based on the location of X-ray detection. Owing to the advantage of Monte Carlo simulation, the trajectory of the incident photon can be readily derived with the knowledge about its position before being detected. The incident trajectory is then projected in the field-of-view planes and the incident angles are further estimated as the angles between the projections and the normal vector of the detector surface. Finally, we estimate the energy deposition in different pixels using the incident angles and plot the X-ray images. Note that the X-ray images presented in this work are vertically reversed and the response function of the XCAM detectors is not considered.

3. Results

Figure 1b shows the comparison of X-ray energy spectra between TERA measurements during event MSE 10-01 and present modeling results. The TERA measurements are obtained from [*Schaal et al.*, 2012]. Present results are calculated by modeling the X-ray production by stepping lightning leaders with two potential drops: 10 MV and 50 MV. The 10 MV leader is assumed to propagate from 376 m altitude to 6 m above the ground with a step length of 10 m, while the 50 MV leader propagates from 376 m altitude to 36 m above the ground with a step length of 20 m. The energy spectra derived without convolution have also been presented to show the effects of the response matrix of unshielded TERA detectors. Although the observed energy spectra correspond to the measurements during only one natural −CG event, TERA data lie well between the two leader potential drops. The spectral hardness in the energy range below 1 MeV is also fairly consistent with TERA measurements. Given the difference at energies above 1 MeV, TERA-measured energy spectra can be best explained using a potential drop between 10 and 50 MV. In order to evaluate the goodness of agreement with observational data for different normalization factors, the least square method is used and the curves shown in Figure 1b are the best fit found. The best agreement with TERA measurements taking into account the detector response is obtained by assuming that $\sim 10^{10}$ photons with energies above 10 keV are produced by the lightning leader with a potential drop of 10 MV. Given these uncertainties, the possible range of number of photons with energy greater than 10 keV produced by the 10 MV leader goes from $\sim 3 \times 10^9$ to $\sim 3.8 \times 10^{10}$.

The comparison of deposited energy with TERA measurements during MSE 10-01 is presented in Figure 1c. The shaded area indicates the uncertainty of the number of

energetic photons produced during the negative corona flash stage of the 10 MV lightning leader. As obtained above through the comparison between modeled and observed spectra, 3×10^9 to 3.8×10^{10} photons with energies above 10 keV are considered to be produced at each step. The solid curve represents the best fit to TERA measurements determined by calculating the sum of squared residuals between natural logarithms of modeling results and observational data. It is obtained by assuming that the 10 MV leader produces $\sim2.2\times10^{10}$ photons with energies above 10 keV, which is consistent, in terms of order of magnitude, with the range assumed by *Celestin et al.* [2015] based on the results reported in [*Saleh et al.*, 2009; *Dwyer et al.*, 2010; *Schaal et al.*, 2012]. This photon number corresponds to a production of $\sim10^{11}$ thermal runaway electrons by the 10 MV leader. Given that the aluminum box outside the TERA detectors and the instrumental effects (e.g., the dead time and pulse pileup effects) are not considered in this work, present results of deposited energy agree in terms of order of magnitude with TERA measurements. We emphasize that the choice of step length determines the total number of leader steps during the stepping process and the total population of bremsstrahlung X-rays produced, and hence the total energy deposition in ground-based detectors. Note that the TERA-measured energy deposition is heavily saturated in the radial distance range between 50 m and 250 m [*Schaal et al.*, 2012]. With the fact of heavy saturation taken into account, the true energy deposition during MSE 10-01 could agree even better with present results.

The left panels of Figure 2 show the positions of X-rays produced by a 10 MV lightning leader at different altitudes corresponding to their last scattering before being detected by an X-ray camera located at (44 m, 0, 0) and, similarly, the right panels show those

for the X-ray camera located at (150 m, 0, 0). The blue square denotes the location of the X-ray camera and the vertical blue line represents the 10 MV lightning leader. This figure illustrates the spatial distribution of X-rays at the locations of their last scattering collisions before being measured by the camera and is derived from Monte Carlo simulations of 5×10^7 photons with energies above 10 keV produced by leader steps in the left panels, while 10^9 photons are used for the right panels. One sees clearly from this figure that photons captured by the camera mainly consist of two groups: unscattered photons originating from the source region in front of the lightning leader tips, and photons recently scattered by air molecules in the region near the detector. Only those scattered photons in the nearby region of the detector can be captured after a single free path because the distance between these photons and the detector is shorter than or comparable to the mean free path.

Modeling results of X-ray images that would be measured using ideal detectors at ground level during the stepping process of a 10 MV lightning leader are presented in Figure 3. The middle panels show X-ray images at the radial distance of 44 m from the lightning ground impact location and the bottom panels show those at 150 m. 2521 m and 8594 m represent the maximum altitudes that the modeled X-ray camera can observe at 44 m and 150 m, respectively. The top panels show the region of the maximum energy deposition in the modeled X-ray images at the radial distance of 44 m. Each panel is a zoom-in view of the X-ray source region with 17×11 pixels (1°×1°). Due to the nonuniform spatial resolution of the modeled X-ray camera, the vertical dimension of each panel, as labeled, is different, although the horizontal dimension is the same (∼13 m). The images are obtained by accumulating all possible X-rays from a given leader step (10^{11} photons with

energy >10 keV are produced per step) at ground level until no photons are present in the simulation. It takes up to a few μs for all the X-rays, emitted after the formation of a new leader step, to be absorbed by the atmosphere, which is much shorter than the time interval between two leader steps. For example, the time interval between typical leader steps is $\sim$24 μs if we consider a step length of 10 m and a leader speed of 4.22×10^5 m/s, as representative of natural $-$CGs [e.g., *Rakov and Uman*, 2003, Table 1.1].

With the difference of angular resolution between the simulated camera and XCAM taken into account, the energy deposition in simulated X-ray images at the radial distance of 44 m is one order of magnitude higher than the XCAM measurements reported in [*Dwyer et al.*, 2011, Figure 8]. The difference is due partly to the longer exposure time used for modeling X-ray images, and partly to the fundamentally different dynamics between triggered lightning discharges and natural $-$CG events. The shielding of XCAM and the detector response are not considered in the present calculation. In addition, we observe that the brightest pixels always locate the X-ray-emitting region, even when the camera is located 150 m away from the lightning discharge.

Apart from this feature, the X-ray images of different leader steps are not self-similar, as better illustrated in those measured at the radial distance of 44 m. First, as the leader descends, the intensity of the brightest pixel is not increasing monotonically, although the distance between the leader tip and the X-ray camera is continuously decreasing. The maximum deposited energy in X-ray images first intensifies from 22 MeV to 47.5 MeV when the leader propagates from 120 m to 40 m, and then drops to 10.5 MeV in the last frame. This quantity is presented separately in Figure 4b. We emphasize that this trend is in line with XCAM observations during triggered lightning discharges [e.g., *Dwyer et al.*,

2011, Figure 8; *Schaal et al.*, 2014, Figure 13]. Second, photons originating from lightning leaders at high altitudes are captured as a bright spot in X-ray images. As the leader propagates downward, the bright spot gradually enlarges and evolves into a half ellipsoid structure. This structure has a width of ∼12 m, comparable to the wide lateral spraying distribution of X-rays measured by XCAM during event UF 11-35 [*Schaal et al.*, 2014, Figure 13].

For a given flux of X-rays produced at the same altitude, the number of collisions that photons undergo is roughly proportional to the distance that they traverse, as shown in Figure 4a. Figure 4a presents the average number of Compton collisions that X-rays produced by leader steps at different altitudes experience before being detected at two locations: 44 m and 150 m away from the lightning ground impact location. One sees, from the results at 44 m, that photons produced by leader steps at relatively higher altitudes would experience more collisions before being registered by detectors at the same radial distance. Likewise, photons originating from leader steps at the same altitude are more severely scattered before arriving at further distances. More Compton scatterings by air molecules result in more energy deposition along the path of X-rays, thereby significantly softening the corresponding energy distribution [e.g., *Xu et al.*, 2014] and reducing the brightness of X-ray images, as evident in Figure 4b. Figure 4b shows the maximum energy deposition in one pixel (with an angular resolution of $1^\circ \times 1^\circ$) produced by leader steps at different altitudes for X-ray images that would be measured at 44 m and 150 m away from the lightning discharge. Besides the difference in intensity, we observe clearly the above-mentioned nonmonotonic behavior of the maximum deposited energy in X-ray images.

4. Discussion

The good agreement obtained between TERA measurements and present modeling results, as shown in Figure 1b, supports the X-ray production mechanism by thermal runaway electrons [*Celestin and Pasko*, 2011]. The number of energetic photons produced by the 10 MV leader, as derived from the comparison with the energy spectrum and deposited energy measured during MSE 10-01, is also consistent with that assumed by *Celestin et al.* [2015] based on the results reported in [*Saleh et al.*, 2009; *Dwyer et al.*, 2010; *Schaal et al.*, 2012]. However, only the TERA measurements during event MSE 10-01 have been investigated. Further comparison with the cumulative energy spectra of X-ray emissions from natural −CG events would provide more insightful information. In the mechanism of X-ray production by thermal runaway electrons, the maximum energy of bremsstrahlung X-rays resulting from stepping leaders is controlled by the potential drop in the leader tip region that is available for thermal runaway electrons. *Celestin et al.* [2015] have revealed the close relation between the potential drop and X-ray energy spectrum: as the potential drop in the vicinity of lightning leader tip increases, the resultant X-ray bursts, as well as the energy spectrum, become more energetic [*Celestin et al.*, 2015, Figure 3]. Based on this relation and the agreement between TERA measurements and the thermal runaway mechanism shown in Figure 1b, we suggest that ground-based X-ray measurements can be used to estimate the approximate range of potential drop of the causative lightning leader.

X-ray images reflect the projection of the spatial distribution of X-rays before being measured in a plane that is parallel to the detector plane. X-rays, before being absorbed by the atmosphere, are mostly distributed in the altitude range below the leader tip, while

a small fraction of them can be backscattered to altitudes even higher than the source. A direct comparison between Figure 2 and Figure 3 shows that unscattered photons lead to the bright spot in X-ray images and the "halo" structure around the bright spot mirrors the spatial distribution of scattered photons. Modeling results suggest that the diffuse emission pattern observed by XCAM could be produced similarly by the detection of heavily scattered photons, i.e., the Compton scattering effects. Nevertheless, at the radial distance of 150 m, this "halo" structure is washed out by the increasing number of Compton scatterings that photons experience and becomes less prominent.

The brightest pixels in X-ray images always pinpoint the source region. For leader steps at low altitudes, unscattered photons dominate the X-ray image and the bright spot illuminates the X-ray-emitting region. For example, the half ellipsoid structure in the X-ray image corresponding to the radial distance of 44 m and the leader altitude of 6 m as shown in Figure 3. As for leader steps at relatively high altitudes, the portion of unscattered photons in X-ray images decreases and the portion of scattered photons increases. The X-ray source region would be slightly broadened by the Compton scattering effects. However, due to the large spatial area of observation for pixels corresponding to high altitudes, this effect is not obvious in the X-ray image.

The energy deposition in the brightest pixel of X-ray images is not changing monotonically. This is because the energy deposition in X-ray images is determined not only by the distance between the source and detectors, but also by the beaming of source photons. As the lightning leader propagates downward, the number of photons that arrive at the X-ray imager first increases due to the reduction of the distance between the source and detectors. This quantity then sharply decreases since the portion of the source photon

beam that is covered by the instrument field of view dramatically reduces. That is, when the lightning leader is close to the ground, which is assumed to be a perfectly absorbing boundary, a significant amount of source photons would reach closer radial distances and only those that are emitted within the observation cone of the X-ray camera can be recorded.

As shown in Figure 3, the diffuse emission pattern as observed in X-ray images during triggered lightning discharges [*Schaal et al.*, 2014] can be explained by the Compton scatterings that X-rays experience. The X-ray source region in front of lightning leader tips would be naturally captured as a compact emission pattern in X-ray images. The emission of bremsstrahlung photons, after being produced by a leader step, into the lower atmosphere is similar to an optical thick target experiment. These photons are heavily scattered by air molecules and a small portion of them could even bounce back to altitudes higher than the source. In this regard, modeling results suggest that the upward moving diffuse glow measured during UF 11-35 [*Schaal et al.*, 2014, Figure 13] is likely due to the back scattering of X-ray bursts by the lower atmosphere. Moreover, results show that X-ray images with higher spatial and energy resolutions would be desirable for the determination of the altitude and size of the X-ray-emitting region, as well as the underlying acceleration processes of energetic electrons.

Appendix A: Detector Response

In this appendix, we describe how the detector response matrix of TERA is used in the calculation of X-ray energy spectra. The convolution of the averaged photon energy distribution with the response matrix of unshielded TERA detectors is performed using the following equation [e.g., *Knoll*, 2010, p. 704]:

$$S(\varepsilon_{\mathrm{i}}) = \frac{\int R(\varepsilon_{\mathrm{i}}, \varepsilon_{\mathrm{p}}) f(\varepsilon_{\mathrm{p}}) d\varepsilon_{\mathrm{p}}}{\Delta\varepsilon_{\mathrm{i}}} \quad (1)$$

where ε_{p} is the energy of the incident photon, ε_{i} is the internal energy of channel i in TERA detectors, $f(\varepsilon_{\mathrm{p}})$ is the spatially averaged energy distribution calculated using Monte Carlo simulations with the unit of $\mathrm{eV}^{-1}\mathrm{m}^{-2}$, $S(\varepsilon_{\mathrm{i}})$ is the X-ray energy spectra in units of $\mathrm{eV}^{-1}\mathrm{m}^{-2}$ that would be measured by TERA detectors, and $R(\varepsilon_{\mathrm{i}}, \varepsilon_{\mathrm{p}})$ is the detector response matrix, which represents the probability that a photon with an energy within $d\varepsilon_{\mathrm{p}}$ of ε_{p} leads to a pulse with an amplitude within $\Delta\varepsilon_{\mathrm{i}}$ of ε_{i}. Specifically, $d\varepsilon_{\mathrm{p}}$ is the energy difference between two adjacent energy grid points used for sampling incident photons and $\Delta\varepsilon_{\mathrm{i}}$ is the energy difference between two internal energy channels (i.e., $\Delta\varepsilon_{\mathrm{i}} = \varepsilon_{\mathrm{i+1}} - \varepsilon_{\mathrm{i}}$). As we see from the comparison shown in Figure 1b, the detector response softens the X-ray energy spectra in the range above ~100 keV.

To calculate the energy deposition presented in Figure 1c, we first convert each photon collected within a given ring into the energy deposition in TERA detectors. The total energy deposition is then divided by the area of the ring in order to compare with TERA measurements. The energy that is deposited into TERA detectors by an incident photon with an energy ε_{p} is calculated using the following formula [*Arabshahi et al.*, 2015]:

$$\varepsilon_{\mathrm{dep}}(\varepsilon_{\mathrm{p}}) = \sum_{\mathrm{i}} R(\varepsilon_{\mathrm{i}}, \varepsilon_{\mathrm{p}}) \varepsilon_{\mathrm{i}} \quad (2)$$

Acknowledgments.

This research was supported by the NSF grants AGS-1106779 and AGS-1243176. Sebastien Celestin's research is supported by the French space agency (CNES) in the frame-

work of the space mission TARANIS. The authors gratefully thank Joseph R. Dwyer, Ningyu Liu, and Shahab Arabshahi for providing the response matrix of TERA detectors. The authors also thank Shahab Arabshahi for the explanation and discussion about the response matrix of TERA detectors. All data used in this paper are directly available after a request is made to authors W.X. (Wei-Xu@colorado.edu), R.A.M. (Robert.Marshall@colorado.edu), S.C. (sebastien.celestin@cnrs-orleans.fr), or V.P.P. (vpasko@psu.edu).

References

Arabshahi, S., et al. (2015), The energy spectrum of X-rays from rocket-triggered lightning, *J. Geophys. Res. Atmos.*, *120*, 10,951–10,963, doi:10.1002/2015JD023217.

Balanis, C. A. (1989), *Advanced Engineering Electromagnetics*, John Wiley, New York.

Bazelyan, E. M., and Y. P. Raizer (2000), *Lightning Physics and Lightning Protection*, Instit. of Phys., Bristol, PA.

Celestin, S., and V. P. Pasko (2011), Energy and fluxes of thermal runaway electrons produced by exponential growth of streamers during the stepping of lightning leaders and in transient luminous events, *J. Geophys. Res.*, *116*, A03315, doi:10.1029/2010JA016260.

Celestin, S., W. Xu, and V. P. Pasko (2012), Terrestrial gamma ray flashes with energies up to 100 MeV produced by nonequilibrium acceleration of electrons in lightning, *J. Geophys. Res.*, *117*, A05315, doi:10.1029/2012JA017535.

Celestin, S., W. Xu, and V. P. Pasko (2015), Variability in fluence and spectrum of high-energy photon bursts produced by lightning leaders, *J. Geophys. Res. Space Physics*, *120*, 10,712–10,723, doi:10.1002/2015JA021410.

Chilingarian, A., et al. (2010), Ground-based observations of thunderstorm-correlated fluxes of high-energy electrons, gamma rays, and neutrons, *Phys. Rev. D*, *82*, 043,009, doi:10.1103/PhysRevD.82.043009.

Dwyer, J. R. (2004), Implications of x-ray emission from lightning, *Geophys. Res. Lett.*, *31*, L12102, doi:10.1029/2004GL019795.

Dwyer, J. R., and D. M. Smith (2005), A comparison between Monte carlo simulations of runaway breakdown and terrestrial gamma-ray flash observations, *Geophys. Res. Lett.*, *32*, L22804, doi:10.1029/2005GL023848.

Dwyer, J. R., D. M. Smith, M. A. Uman, Z. Saleh, B. Grefenstette, B. Hazelton, and H. K. Rassoul (2010), Estimation of the fluence of high-energy electron bursts produced by thunderclouds and the resulting radiation doses received in aircraft, *J. Geophys. Res.*, *115*, D09206, doi:10.1029/2009JD012039.

Dwyer, J. R., M. Schaal, H. K. Rassoul, M. A. Uman, D. M. Jordan, and D. Hill (2011), High-speed X-ray images of triggered lightning dart leaders, *J. Geophys. Res.*, *116*, D20208, doi:10.1029/2011JD015973.

Dwyer, J. R., D. M. Smith, and S. A. Cummer (2012), High-energy atmospheric physics: Terrestrial gamma-ray flashes and related phenomena, *Space Sci. Rev.*, *173*, 133–196, doi:10.1007/s11214-012-9894-0.

Dwyer, J. R., et al. (2003), Energetic radiation produced during rocket-triggered lightning, *Science*, *299*, 694–697, doi:10.1126/science.1078940.

Dwyer, J. R., et al. (2004), Measurements of x-ray emission from rocket-triggered lightning, *Geophys. Res. Lett.*, *31*, L05118, doi:10.1029/2003GL018770.

Dwyer, J. R., et al. (2005), X-ray bursts associated with leader steps in cloud-to-ground lightning, *Geophys. Res. Lett.*, *32*, L01803, doi:10.1029/2004GL021782.

Gurevich, A. V., G. M. Milikh, and R. A. Roussel-Dupré (1992), Runaway electron mechanism of air breakdown and preconditioning during a thunderstorm, *Phys. Lett. A.*, *165*(5–6), 463–468, doi:10.1016/0375-9601(92)90348-P.

Knoll, G. F. (2010), *Radiation Detection and Measurement*, 3rd ed., John Wiley, Hoboken, N. J.

Moore, C. B., K. B. Eack, G. D. Aulich, and W. Rison (2001), Energetic radiation associated with lightning stepped-leaders, *Geophys. Res. Lett.*, *28*(11), 2141–2144, doi:10.1029/2001GL013140.

Moss, G. D., V. P. Pasko, N. Liu, and G. Veronis (2006), Monte Carlo model for analysis of thermal runaway electrons in streamer tips in transient luminous events and streamer zones of lightning leaders, *J. Geophys. Res.*, *111*, A02307, doi:10.1029/2005JA011350.

Østgaard, N., T. Gjesteland, J. Stadsnes, P. H. Connell, and B. Carlson (2008), Production altitude and time delays of the terrestrial gamma flashes: Revisiting the Burst and Transient Source Experiment spectra, *J. Geophys. Res.*, *113*, A02307, doi:10.1029/2007JA012618.

Qi, Q., W. Lu, Y. Ma, L. Chen, Y. Zhang, and V. A. Rakov (2016), High-speed video observations of the fine structure of a natural negative stepped leader at close distance, *Atmos. Res.*, *178*, 260–267, doi:10.1016/j.atmosres.2016.03.027.

Rakov, V. A., and M. A. Uman (2003), *Lightning: Physics and Effects*, Cambridge Univ. Press, Cambridge, U. K.

Saleh, Z., J. Dwyer, J. Howard, M. Uman, M. Bakhtiari, D. Concha, M. Stapleton, D. Hill, C. Biagi, and H. Rassoul (2009), Properties of the X-ray emission from rocket-triggered lightning as measured by the Thunderstorm Energetic Radiation Array (TERA), *J. Geophys. Res.*, *114*, D17210, doi:10.1029/2008JD011618.

Schaal, M. M., J. R. Dwyer, Z. H. Saleh, H. K. Rassoul, J. D. Hill, D. M. Jordan, and M. A. Uman (2012), Spatial and energy distributions of X-ray emissions from leaders in natural and rocket triggered lightning, *J. Geophys. Res.*, *117*, D15201, doi: 10.1029/2012JD017897.

Schaal, M. M., et al. (2014), The structure of X-ray emissions from triggered lightning leaders measured by a pinhole-type X-ray camera, *J. Geophys. Res. Atmos.*, *119*, 982–1002, doi:10.1002/2013JD020266.

Tran, M. D., V. A. Rakov, and S. Mallick (2014), A negative cloud-to-ground flash showing a number of new and rarely observed features, *Geophys. Res. Lett.*, *41*(18), 6523–6529, doi:10.1002/2014GL061169.

Xu, W., S. Celestin, and V. P. Pasko (2012), Source altitudes of terrestrial gamma-ray flashes produced by lightning leaders, *Geophys. Res. Lett.*, *39*, L08801, doi: 10.1029/2012GL051351.

Xu, W., S. Celestin, and V. P. Pasko (2014), Modeling of X-ray emissions produced by stepping lightning leaders, *Geophys. Res. Lett.*, *41*, 7406–7412, doi: 10.1002/2014GL061163.

Xu, W., S. Celestin, and V. P. Pasko (2015), Optical emissions associated with terrestrial gamma ray flashes, *J. Geophys. Res. Space Physics*, *120*, 1355–1370, doi: 10.1002/2014JA020425.

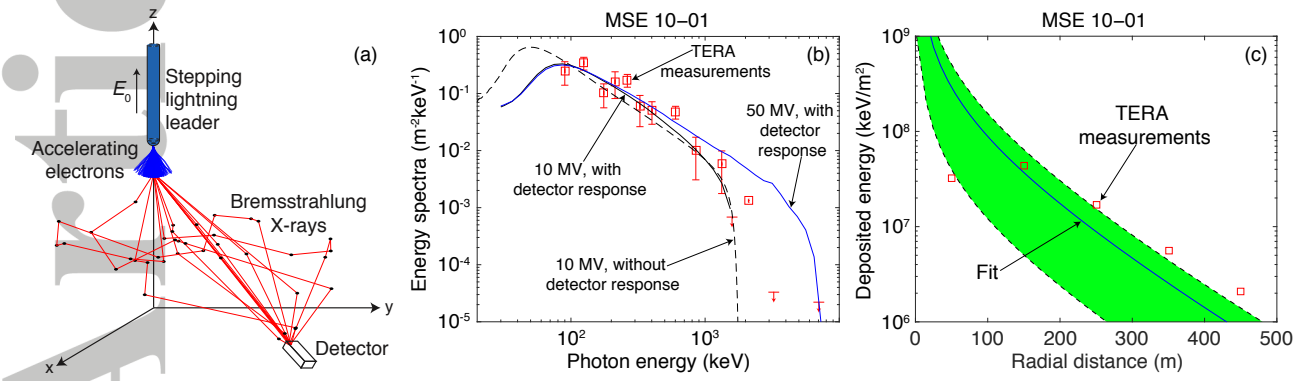

Figure 1. (a) Sketch of the simulation domain used for modeling X-ray images. (b) Comparison of X-ray energy spectra between TERA measurements during event MSE 10-01 and present modeling results. The results are obtained by modeling the X-ray production during the stepping process of lightning leaders with two potential drops: 10 MV and 50 MV. (c) Comparison of deposited energy between TERA measurements during event MSE 10-01 and present modeling results. The solid curve represents the best fit to TERA measurements and the shaded area indicates the range of photon number produced by the 10 MV lightning leader as estimated from the comparison of X-ray energy spectrum. TERA measurements are obtained from [*Schaal et al.*, 2012].

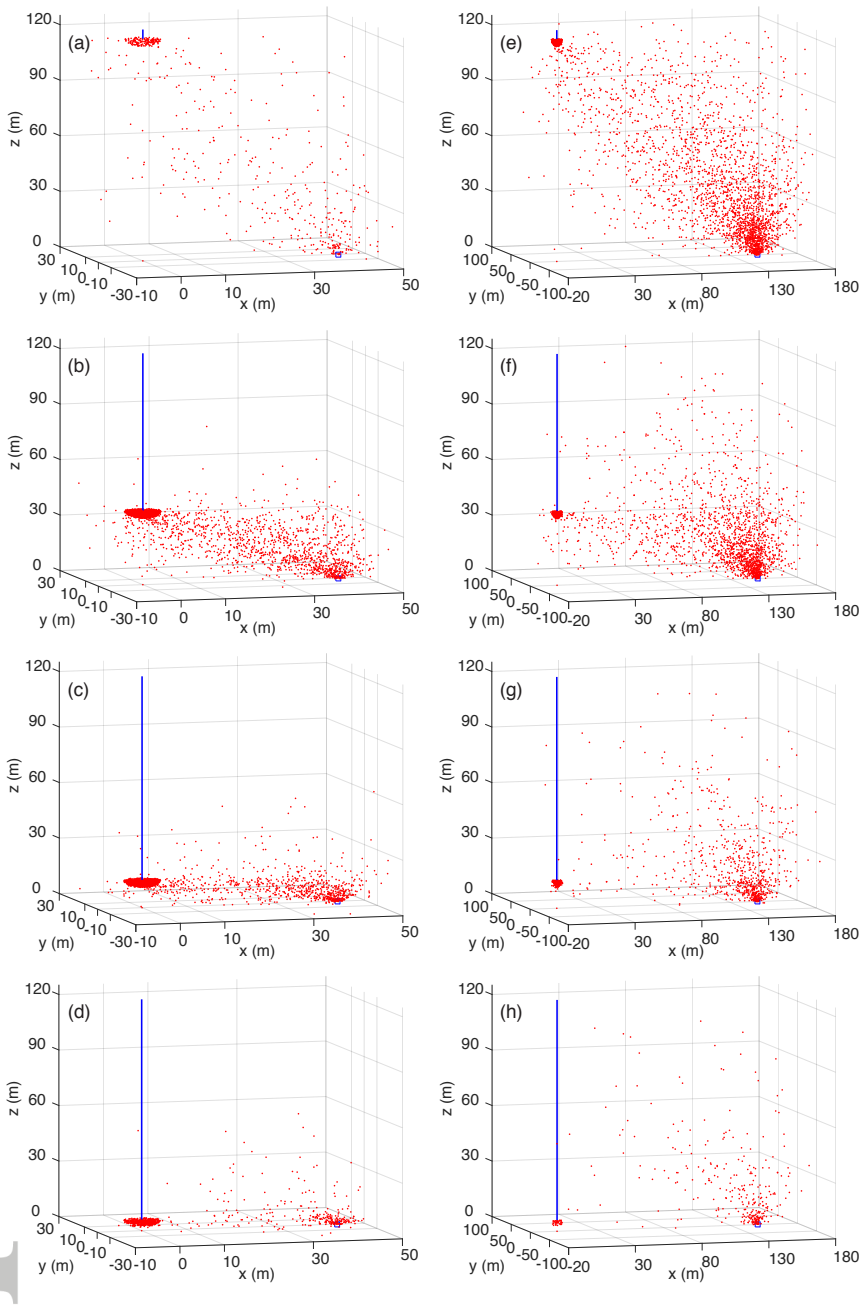

Figure 2. Last scattering positions of X-rays produced by a 10 MV lightning leader at (a) 120 m, (b) 40 m, (c) 15 m, and (d) 6 m altitude before being measured by an X-ray camera located at (44 m, 0, 0). Last scattering positions of X-rays produced by a 10 MV lightning leader at (e) 120 m, (f) 40 m, (g) 15 m, and (h) 6 m altitude before being measured by an X-ray camera located at (150 m, 0, 0). The blue square denotes the location of the modeled X-ray camera and the vertical blue line represents the 10 MV lightning leader.

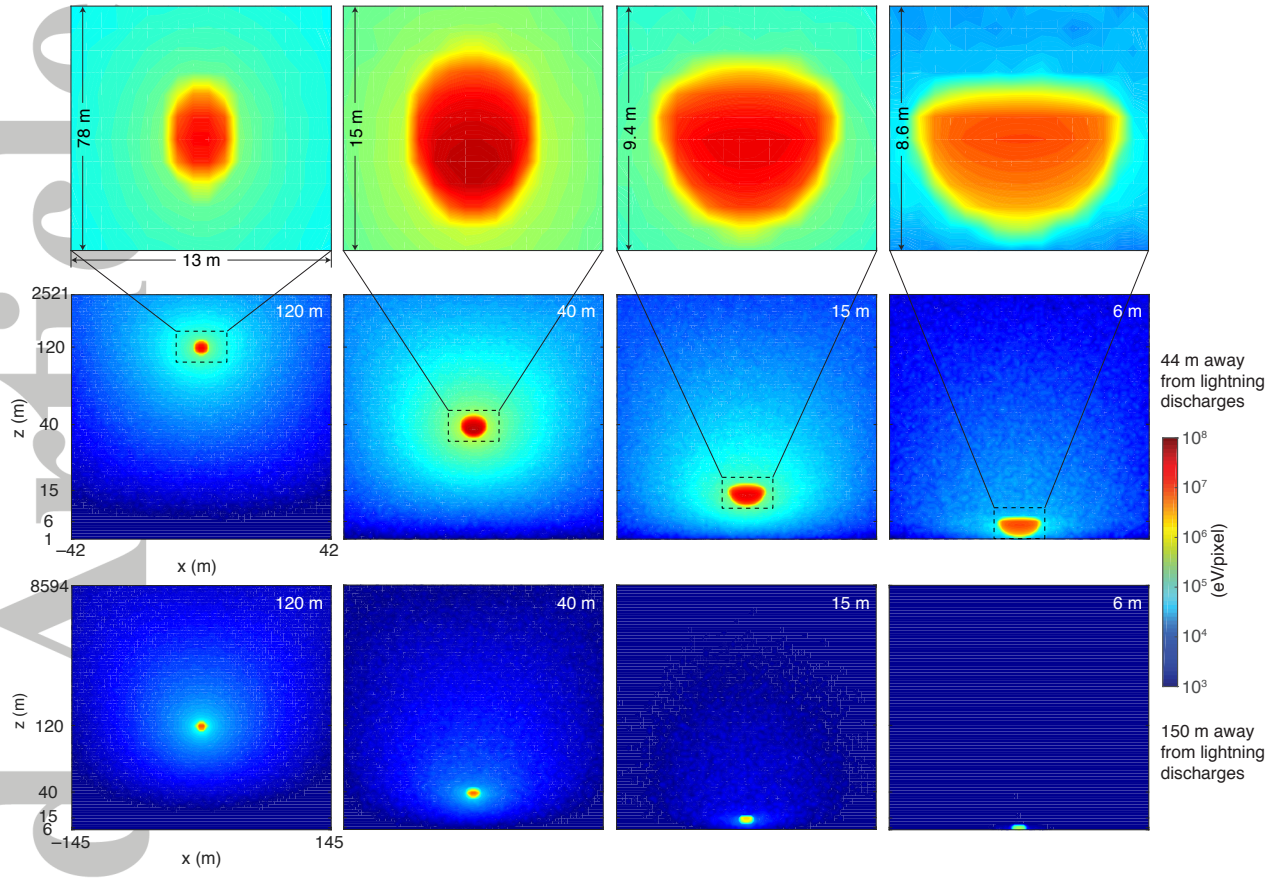

Figure 3. X-ray images that would be measured using ideal detectors at ground level during the stepping process of a 10 MV lightning leader. The middle panels show the X-ray images at a radial distance of 44 m from the lightning ground impact location and the bottom panels show those at 150 m. The altitudes of leader steps are labeled in the upper right corner of each panel. The top panels are the zoom-in view, with 17×11 pixels, of the X-ray source region in the modeled X-ray images at the radial distance of 44 m. The elevation angle of the X-ray camera is 45° and the instrument field of view is ±44° in both vertical and horizontal directions with an angular resolution of 1°×1°. Note that the response function of XCAM detectors is not considered.

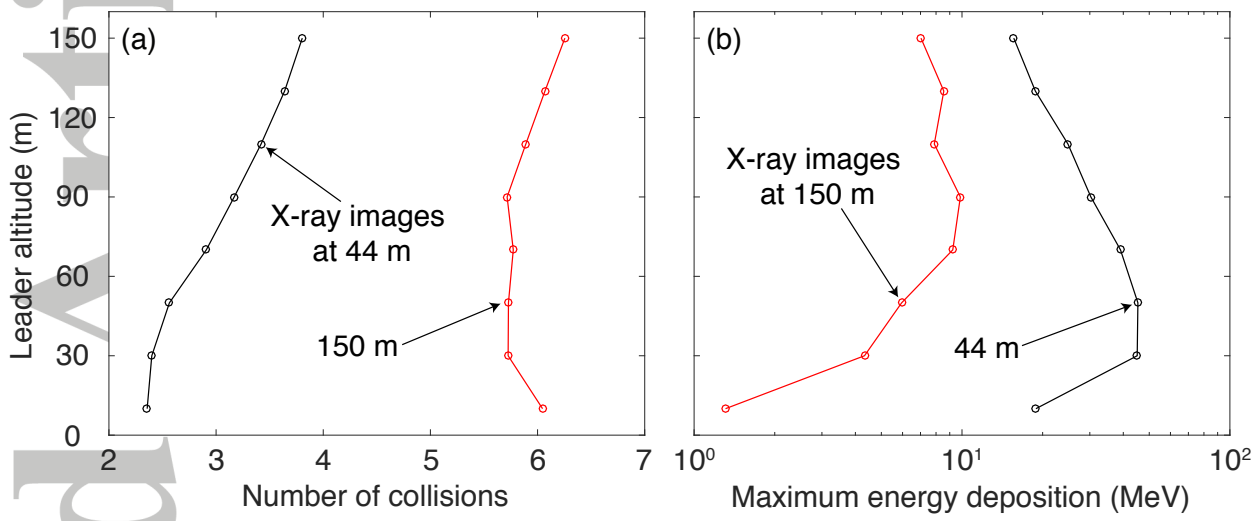

Figure 4. (a) Average number of collisions that X-rays produced by leader steps at different altitudes experience before being detected at two locations: 44 m and 150 m away from the lightning ground impact location. (b) Maximum energy deposition in one pixel (with an angular resolution of $1^\circ \times 1^\circ$) produced by leader steps at different altitudes for X-ray images that would be measured at two locations: 44 m and 150 m away from the lightning ground impact location.